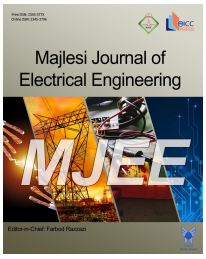

Volume 19, Issue 1, 192515 (1-15)

Majlesi Journal of Electrical Engineering (MJEE)

https://doi.org/10.57647/j.mjee.2025.1901.15

Genetic algorithm-based control strategies for efficient residential DC microgrid systems with hybrid storage

Amit Kumar Rajput*, Jagdeep Singh Lather

Department of Electrical Engineering, National Institute of Technology, Kurukshetra, India.

***Corresponding author:** gowidrajput@gmail.com

Original Research

Received:
25 November 2024
Revised:
14 January 2025
Accepted:
29 January 2025
Published online:
1 March 2025

Abstract:

This paper presents a power management and control strategy for a residential DC microgrid (DCMG) incorporating photovoltaic (PV) systems, fuel cells (FCs), and a hybrid energy storage system (HESS). The fluctuations in the DC bus voltage, arising from intermittent PV generation and variable load conditions, are mitigated by the HESS, which comprises both batteries and supercapacitors (SCs). This control strategy adopts, batteries to handle slow-frequency power surges, whereas SCs are employed to manage rapid frequency fluctuations effectively. The proposed controllers are optimized using an evolution-based Genetic Algorithm (GA), eliminating the need for extensive mathematical modeling of the system. Comparative analysis between the GA-tuned and conventionally tuned controllers is conducted based on performance metrics, including overshoot, undershoot, and settling time. The simulation results indicate that the proposed controller performs satisfactorily, achieving a maximum overshoot of 3.08%, a maximum undershoot of 2.95%, and a settling time of 44.5 ms. To further assess the efficacy and robustness of the controllers, they are subjected to disturbances in sensor readings and variations in system parameters within a range of ±25% of their nominal values. Additionally, to validate the practical applicability of the proposed system, the simulation results are corroborated using a real-time FPGA-based simulator (OP 5700).

Keywords: Photovoltaic; Fuel cell; Battery; Supercapacitor; Energy management; Genetic algorithm

1. Introduction

1.1 Motivation

Energy demands have witnessed steep rise owing to continued modernization and industrialization across the globe. As conventional energy resources are depleting rapidly, there is a growing need to supplement them with renewable energy sources (RESs) to meet energy demands. The natural shift toward RESs alleviates harmful environmental impacts, such as global warming and rising sea levels, by decarbonizing the power sector—a problem so severe that low-lying countries, like the Maldives, are fighting to preserve their very existence [1, 2]. Microgrids (MGs) have emerged as a highly efficient alternative to traditional power systems, characterized by their decentralized nature and integration of RESs and energy storage systems (ESSs), offering sustainable and resilient energy solutions, particularly for remote locations. A MG can be AC, DC, or a hybrid AC-DC, though DCMGs are particularly favored by the scientific and research communities due to their inherent advantages and ease of control.

DC systems provide superior voltage control, as they eliminate reactive power, reduce power losses during capacitor charge/discharge, and allow the use of thinner conductors due to the absence of skin effect. Additionally, they are more efficient due to fewer conversion stages [3–5]. With rapid advancements in DC technologies and the growing penetration of DC loads, such as digital devices, mobile communications, and electric vehicles, DCMGs represent a promising solution for the future of smart grids [6, 7]. The general layout of a DCMG consisting of distributed generators (DGs), DC loads and ESSs is shown in figure 1. DCMGs incorporating PV and wind systems as DGs are gaining popularity due to their portability, scalability, and cost-effectiveness compared to other RESs. However, designing an effective controller for DCMGs poses significant challenges, including maintaining balanced states of charge (SoCs) and addressing power imbalances, both of which are further complicated by the inherent variability of wind and solar irradiance. To mitigate these issues and ensure a stable power supply, ESSs, typically batteries, are commonly used. While batteries are effective for energy storage, their low power density limits their ability to meet instantaneous

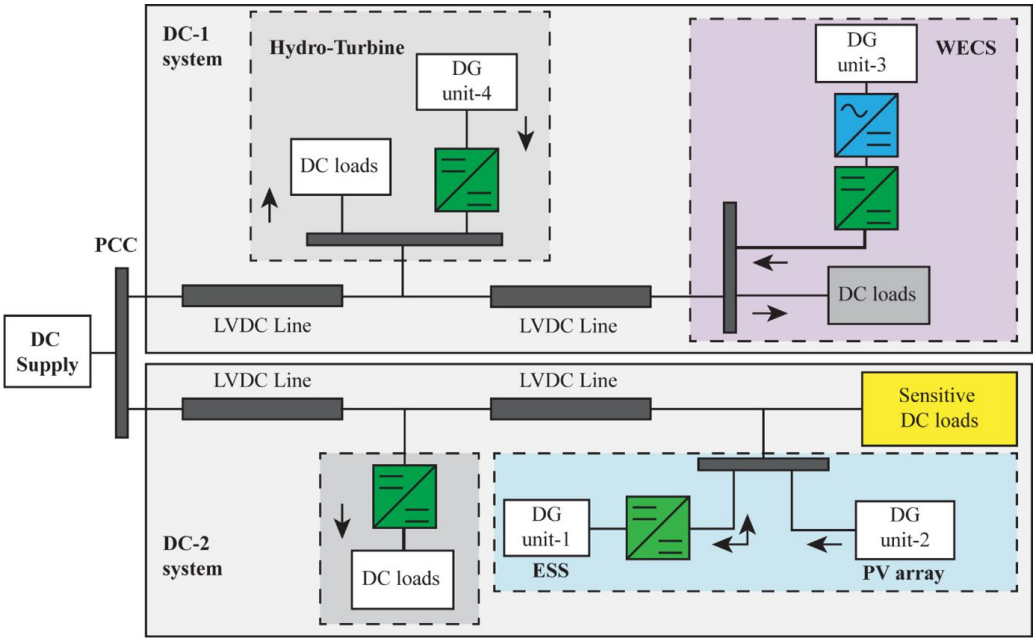

Figure 1. General layout of DC microgrid.

power demands [8, 9]. To overcome this limitation, SCs, with their high-power density, are often paired with batteries to manage both slow and dynamic load variations, as well as disturbances from PV fluctuations. This integration is referred to as hybrid energy storage systems (HESSs), which improve the overall reliability and performance of DCMGs in managing variable energy inputs and load demands. In HESSs, batteries are tasked with meeting high energy demands, while SCs address high power requirements. SCs not only help stabilize MG by smoothing out power transients but also improve battery performance and longevity by reducing ripple in the DC bus voltage [10]. Despite these advantages, PV-HESS systems alone may struggle to provide consistent power during prolonged periods of unfavorable weather, leading to potential blackouts. To resolve this issue, dispatchable energy resources such as FCs are often integrated with PV systems to ensure reliable power generation. In this work, we consider a DCMG configuration that incorporates a PV system, FCs, and a HESS composed of both batteries and SCs, aiming to enhance the system's resilience and stability under varying environmental conditions.

Nomenclature

η_{act} activation overvoltage (V)

V_{DC} actual DC bus voltage (V)

A amplitude of voltage in exponential zone (V)

C_{Ah} battery capacity (Ah)

E_{Bat} battery voltage (V)

E_0 constant voltage of battery (V)

I_m current of PV module at maximum power point (A)

C_{DC} DC bus capacitance (F)

Q_T electric charge (in C)

B exponential zone time constant inverse (Ah^{-1})

i^* filtered current (A)

V_{FC} fuel cell voltage (V)

I_T^* gross current (A)

L_{Bat} inductance of battery's BDC (H)

L_{FC} inductance of fuel cell's boost converter (H)

L_{pv} inductance of PV's boost converter (H)

L_{SC} inductance of supercapacitor's BDC (H)

K_{i_B} integral gain of battery's current control loop

K_{i_SC} integral gain of supercapacitor's current control loop

K_{i_v} integral gain of supercapacitor's voltage control loop

A_i interfacial area between electrodes and electrolytes (in m^2)

Q max. battery capacity (Ah)

E_{FC} nernst voltage (V)

N_e number of electrode layers

N_0 number of cells connected in series

N_s number of SC in series

N_p number of SCs in parallel

η_{ohm} Ohmic overvoltage (V)

E_0 open circuit voltage of FC (V)

V_{oc} open circuit voltage of PV module (V)

ρ_{H_2} partial pressure of hydrogen (atm)

ρ_{O_2} partial pressure of oxygen (atm)

ρ_{H_2O} partial pressure of water (atm)

ε permittivity of material

K polarization constant (Ah^{-1})

K_{p_B} proportional gain of battery's current control loop

K_{p_sc} proportional gain of supercapacitor's current control loop

K_{p_v} proportional gain of supercapacitor's voltage control loop

V^*_{DC} reference DC bus voltage (V)

I_{SC} short circuit current of PV module (A)

T temperature (in K)

V_T terminal voltage of an SC (V)

R universal gas constant

V_m voltage of PV module at maximum power point (V)

1.2 Literature

Fengyan Zhang et al. [11] proposed an energy management strategy (EMS) in a grid-dependent DCMG incorporating PV and HESS, with a control strategy divided into four modes and seven sections based on the DC bus voltage range. However, this strategy does not effectively regulate the DC bus voltage during the transition phase. Chaouali et al. [12] introduced a power management strategy (PMS) for a DCMG integrating PV, FC, and SC technologies to supply power to a pumping station. The proposed control strategy leverages a fuzzy logic control technique to optimize system performance. Abeywardana et al. [13] presented a grid-connected DCMG configuration comprising PV and a sliding mode-controller (SMC) based HESS, with the overall system demonstrating robustness to certain model parameters and uncertainties. However, the authors did not address the steps necessary to mitigate chattering in the control system. Maheswari et al. [14] proposed a control strategy to maintain the demand-generation balance in a PV-HESS based DCMG. The HESS effectively mitigates intermittent fluctuations in PV power, contributing to enhanced battery life as a result of the overall strategy. Similarly, to address the intermittency issues in renewable-based MGs, Zhou et al. [15] proposed the integration of a HESS in conjunction with dual active bridges. Athira et al. [16] proposed a fuzzy logic-based PMS for a standalone DCMG utilizing PV, battery, and SC systems, with the strategy regulating SoC of both the battery and SC within predefined upper and lower boundaries. However, the overall approach is contingent upon historical system information used in the design of the fuzzy-based PMS. Han et al.[17] proposed a DCMG model utilizing the PV, FC and battery in a coordinated manner to address balance in demand and generation. However, their approach does not account for the issue of DC bus voltage regulation (VR). Similarly, Pu et al. [18] introduced a hierarchical control scheme for a DCMG comprising of PV, FC, battery and loads, with a primary focus on minimizing utilization costs. However, their strategy also fails to consider power-sharing among the various modules and regulation of the DC bus voltage. Cabrane et al. [19] proposed a control strategy using HESS to flatten out fluctuation in PV power generation. HESS not only provides smoother traction system management but also decreases stress on the battery in transient conditions, extending its life. Following this research, Cabrane et al. [20] further developed an EMS for a similar MG configuration but without inclusion of FC. This study included a detailed comparison of various battery-SC topologies and examined the impact of filter time constants on both the battery and the SC. Wang et al. [21] presented a control scheme for a DCMG based on DESs and HESS. The HESS improves the utilization of ESSs and stabilizes the DCMG operation. However, the DC bus VR is not addressed. In contrast, Wen et al. [22] proposed a control strategy based on multiple operating states of battery's SoC. This approach divides the battery's SoC into various sections to prevent excessive depth of charge/discharge, thereby optimizing the operating life of ESS.

Senapati et al. [23] proposed an enhanced power management and control strategy for a DCMG, focusing on improving the dynamics of DC link voltage and optimizing power distribution among connected units. They utilized a gain control technique for grid-side management and implemented a dynamically tuned PI controller for battery energy storage, employing Takagi-Sugeno fuzzy logic to enhance the transient voltage response. In a related study [24], they developed an enhanced MPP tracking algorithm by combining P&O method with a modified invasive weed optimization (MIWO) algorithm. This hybrid approach improved convergence speed and GMPP accuracy under fluctuating climatic conditions, outperforming existing techniques like GWO with FLC and modified butterfly optimization algorithm (MBOA). Robustness was validated through small signal analysis, confirming its effectiveness across various scenarios. In subsequent work, Senapati et al. [25, 26] introduced a Firefly Algorithm-based Particle Swarm Optimization (FA-PSO) control strategy for a standalone DCMG, aiming to achieve faster DC-link voltage control and optimal power balancing. They further refined the controller design by incorporating techniques such as Takagi-Sugeno fuzzy logic, Grey Wolf Optimization (GWO), and Adaptive Neuro-Fuzzy Inference System (ANFIS) assisted by PSO. Ultimately, they compared the performance of these methods, demonstrating the superiority of the FA-PSO-based controller.

Singh and Lather [27] proposed a control scheme for energy management in a grid-independent DCMG that utilizes a HESS. In their approach, the controller is tuned using frequency domain analysis through a transfer function method, achieving a maximum voltage deviation of 4.18% in DC bus. Rajput and Lather [28] proposed an EMS for an autonomous DCMG that employs a HESS using a combination of proportional-integral (PI) and Artificial Neural Network

(ANN) controllers. Their MG configuration features a semi-active HESS, where the battery is managed through a power electronics converter, while SC is directly connected to the DC bus. However, this arrangement leads to the oversizing of the SC, resulting in inefficient utilization of the SC. Pavkovic et al. [29] proposed cascade control system and adaptive load compensation for a DCMG. However, the controller exhibited slower response times and struggled to effectively regulate the DC bus voltage. In contrast, a controller design utilizing magnitude and symmetric optimum criteria was introduced in [30, 31], but the system response was suboptimal when disturbances occurred beyond the reference input. Additionally, the symmetric optimum criterion demonstrated significant overshoots. On the other hand, Fan et al. [32] proposed automatic tuning method for a PID controller using Genetic Algorithm (GA). Their results were compared with those obtained from Ziegler-Nichols and fuzzy-tuned PID controllers, showing that the GA-tuned controller outperformed the others in terms of both static and dynamic characteristics. Kumar et al. [33] employed GA to manage power flow control in a grid-connected distributed system, focusing on controlling both active and reactive power. Their control strategy demonstrated the effectiveness of the proposed model under both balanced and unbalanced power supply conditions, ensuring that the output of all power sources remain stable, and the overall system maintained its stability.

Considering the aforementioned issues and perspectives into account, this paper proposes a control and energy management system for an autonomous DCMG with a HESS, in which the controllers are optimized for peak performance using GA.

1.3 Contribution

This work proposes a PMS for a residential DCMG that integrates RES and a HESS to ensure reliable operation under all weather conditions. The innovative contributions presented in this article are as:

- Effective regulation of DC bus voltage, maintaining it within strict limits of ±5% in accordance with IEEE standard 519-1992.
- Effective power sharing among various units of DCMG irrespective of variability in weather conditions and load cycle.
- Enhanced regulation of SoC for both the battery and SC, ensuring they remain within the desired range to prevent overcharging and deep discharging.
- Optimal gains for PI controllers using GA to enhance overall system performance.

1.4 Organization

The rest of the paper is organized as follows: section 2 highlights system configuration and its modeling. Section 3 discusses GAs and GA-based controller design. Section 4 illustrates the proposed controller and PMS. Section 5 presents simulation results, in-depth analysis, and comparison with a conventional controller, while section 6 discusses experimental results using Opal-RT. Section 7 focuses on the sensitivity analysis of the proposed controller, and section 8 evaluates the controller's performance in the presence of sensor noise. Finally, section 9 discusses potential avenues for future research, and section 10 presents conclusion of the study.

2. DCMG system configuration and modeling

Figure 2 shows the considered standalone DCMG configuration, consisting of PV as main generating source, FC, and HESS as a buffer for DC bus VR. The PV and FCs are connected to the DC bus through boost converters, while the battery and SCs are linked via bidirectional DC-DC converters (BDCs), with the duty cycle for these converters generated by controllers to regulate deviations in DC bus voltage.

The sun irradiation data for NIT, Kurukshetra, Haryana, India (29.9476 °N, 76.8155 °E) is obtained from NASA's Surface Meteorology database. The solar energy data confirms the suitability of the location for the deployment of PV-based MGs. It is evident from figure 3; the selected site receives ample solar radiation with an averaging of 5.6 kWh/m^2/day and a clearness index of 0.55 on monthly basis.

2.1 Mathematical modeling of PV cell

The one-diode model of PV cell, as shown in figure 4, is adopted for this research work [5]. V-I characteristics for the one diode model of PV cell can be expressed as

$$I = I_{\mathrm{PV}} - I_0\left[\exp\left(\frac{V+IR_s}{nV_t}\right)-1\right] - \frac{V+IR_s}{R_p} \qquad (1)$$

2.2 Mathematical modeling of FC

Unlike batteries, FCs are a consistent source of power in proportion to available fuel. Voltage of the FC using polar-

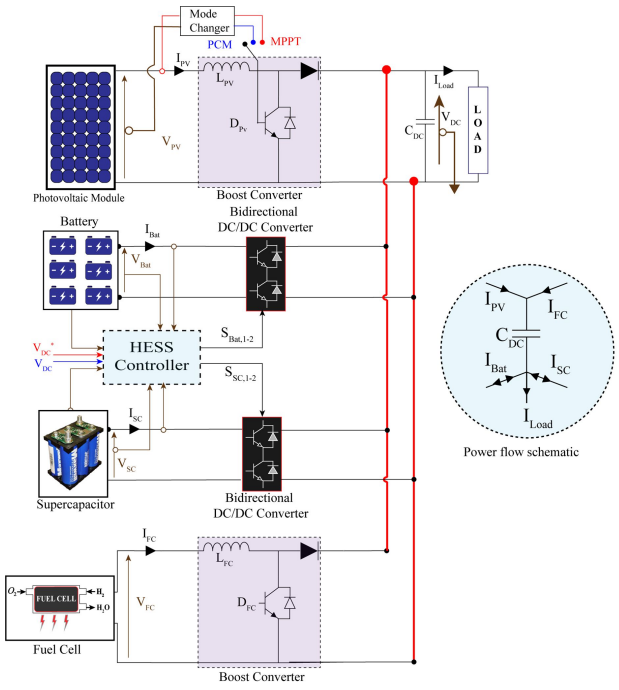

Figure 2. Proposed DC microgrid configuration.

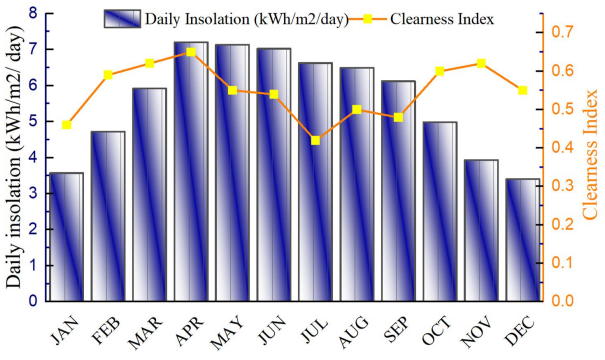

Figure 3. Solar isolation and clearness index at NIT, Kurukshetra, Haryana, India.

ization curve can be expressed as [34]

$$V_{FC} = E_{FC} + \eta_{act} + \eta_{ohm} \tag{2}$$

where, Nernst voltage (E_{FC}) is thermodynamic voltage of the cells that can be expressed as

$$E_{FC} = N_0 \left[E_0 + \frac{RT}{2F} \log \left[\frac{\rho_{H_2} \rho_{O_2}^{0.5}}{\rho_{H_2O}} \right] \right] \tag{3}$$

2.3 Mathematical modeling of battery

The battery serves as a buffer, ensuring consistent and flawless bus voltage functioning regardless of demand-generation mismatch. The use of batteries also boosts RESs utilization. The selection of suitable battery capacity is critical in determining the longevity of battery operation for a certain load. To decide the battery capacity (C_{Ah}), initial battery SoC is considered 50%. Battery capacity is calculated in such a way that it could fulfil the energy demand of 3.5 kW load for an hour.

Battery capacity can be calculated as [35]

$$C_{Ah} = \frac{3.5\ \text{kW} \times 1\ \text{h}}{24\ \text{V} \times 0.5} \cong 292\ \text{Ah} \tag{4}$$

Figure 5 shows the equivalent circuit of the battery, which is modeled as a resistance in series with a constant voltage source. The charging and discharging processes of the battery are characterized as [36]

Charge equation ($i^* < 0$) for Lithium-Ion battery

$$E_{Bat} = E_0 - K \cdot \frac{Q}{it + 0.1Q} \cdot i^* - K \cdot \frac{Q}{Q - it} \cdot it + A \cdot \exp(-B \cdot it) \tag{5}$$

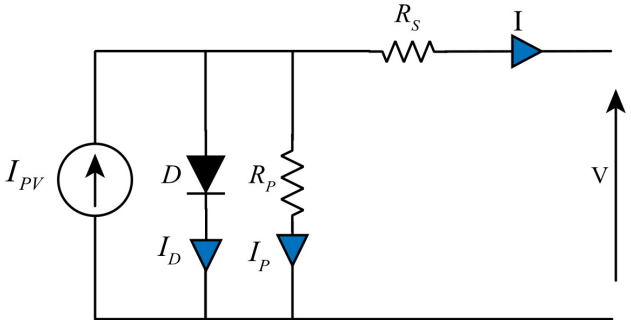

Figure 4. Equivalent circuit of a PV cell.

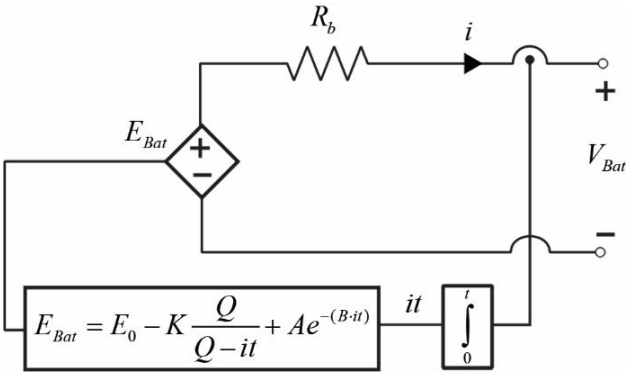

Figure 5. Equivalent circuit of battery.

Discharge ($i^* > 0$) equation,

$$E_{Bat} = E_0 - K \cdot \frac{Q}{Q - it} \cdot i^* - K \cdot \frac{Q}{Q - it} \cdot it + A \cdot \exp(-B \cdot it) \tag{6}$$

2.4 Mathematical modeling of SC

The SC model based on stern principle as shown in figure 6, is used to imitate the characteristics of SC [37]. Accordingly, the terminal voltage of an SC is expressed as

$$V_T = \frac{N_s Q_T d}{N_p N_e \varepsilon \varepsilon_0 A_i} + \frac{2N_e N_s RT}{F} \sinh^{-1}\left(\frac{Q_T}{N_p N_e^2 A_i \sqrt{8RT\varepsilon\varepsilon_0 c}} \right) - R_{SC} \cdot i_{SC} \tag{7}$$

with

$$Q_T = \int i_{SC} dt \tag{8}$$

and, SoC of SC can be calculated as

$$\text{SoC}_{SC} = \frac{Q_{init} - \int_0^\tau i(\tau) d\tau}{Q_T} \times 100 \tag{9}$$

Parameters for the proposed microgrid configuration are tabulated in Table 1.

3. Optimization of controller

3.1 PID controller tuning

PID controllers are one of the most commonly used in industrial applications, owing to their simplicity, robustness, adaptability, and the capacity for online retuning [38]. PID controllers consist of three distinct terms named as proportional, integral, and derivative. Each of them has a specific

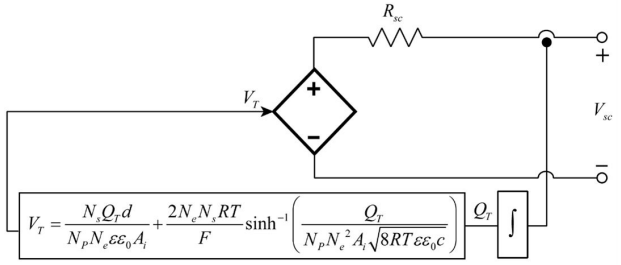

Figure 6. Electrical equivalent of SC.

Table 1. Selected parameters of DC microgrid.

PV array @ STC	$V_{OC} = 32$ V, $I_{SC} = 7.6$ A, $V_m = 26$ V, $I_m = 6.8$ A
proton exchange membrane FC	24 V, 1.26 kW
battery	24 V, 292 Ah
supercapacitor	29 F, 32 V
DC-DC converters	$L_{SC} = 1.8$ mH, $L_{Bat} = 2$ mH, $L_{pv} = 13.25$ mH, $L_{FC} = 4$ mH, $C_{DC} = 440$ μF
controller [K_{p_B}, K_{i_B}, K_{p_sc}, K_{i_sc}, K_{p_v}, K_{i_v}]	[0.9, 2500, 20, 3200, 0.95, 850]

impact on the plant, depending on error $e(t)$. Overall control function of controller can be written as

$$u(t) = K_p e(t) + K_I \int_0^t e(t)dt + K_D \frac{de(t)}{dt} \tag{10}$$

where K_p, K_I and K_D are proportional, integral, and derivative gains, and $e(t)$ denotes the error between the input (set point) and the output, these PID controllers can be tuned using both classical methods like Ziegler-Nichols and Cohen-Coon, as well as more modern computational or optimization techniques, offering flexibility in finding the right balance for various control systems. However, PID controllers are widely tuned using traditional techniques, but these methods do not always yield the desired results, often requiring further adjustments [39–41]. Here, PI controllers are designed to meet system requirements and K_D is considered as zero. Fine tuning PI controller using optimization-based procedures improves the system response in terms of rise time, overshoot, and settling time [42]. In this work, GA-based PI controller enhancement strategy is developed to optimize performance.

3.2 Genetic algorithm

GA is a simple, robust and probabilistic global search method that mimics natural biological evolution based on the survival of the fittest and produces closer approximations to a solution with each evolution. Best individuals are selected based on their level of fitness to generate and breed new offspring within the problem domain. The fitness level of the individuals involved is assessed based on the objective function. The evaluation of this fitness is conducted using time-integrated performance indices, which include the integral of absolute error (IAE), the integral of squared error (ISE), and the integral of time-weighted absolute error (ITAE). To achieve satisfactory dynamic performance, minimization of the ITAE is selected as the performance index, expressed as follows:

$$J = \sum_{n=1}^{3} \left(\int_0^{\infty} t|e_n(t)|dt \right) \tag{11}$$

where $e_n(t)$ denotes the difference between actual and set point value of nth PI controller. Three PI controllers used for HESS are tuned and optimized using GA. Time (t) weighing is used to scale down the large initial error in the suitable range. Figure 7 (a) shows the fitness value of each

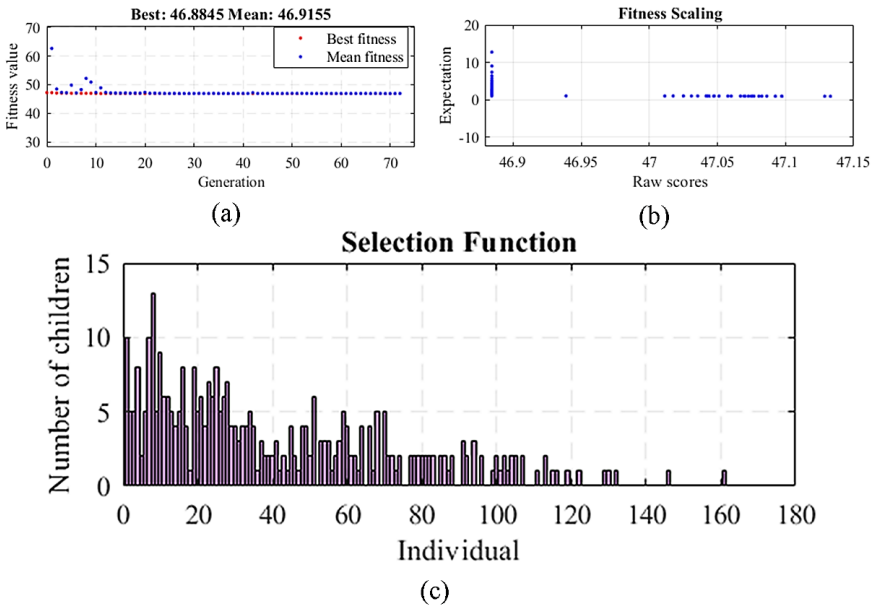

Figure 7. GA optimization results (a) Fitness value for each generation (b) Fitness scaling (c) Selection function.

generation wherein it is depicted that the best function value is 46.8845 and mean is 46.9155.

The raw fitness scores produced by the fitness function are adjusted through a scaling process to fit within a value range suitable for the selection function. The selection function utilizes these scaled fitness values to identify the parents for the next generation. According to this selection process, individuals with higher scaled scores have a greater probability of being chosen as parents. The fitness scaling plot depicted in figure 7 (b) employs the rank method. This approach scales raw scores according to their rank rather than their actual values. The scaled value of an individual with rank n is inversely proportional to $1/\sqrt{n}$.

The average performance of offspring improves as better individuals are preserved for mating while less fit individuals die out. To generate the new offspring, a population has to go through various stages such as selection, crossover and mutation. Various selection techniques are available in GA, such as tournament selection, roulette wheel selection, and rank selection; however, tournament selection has proven to be superior in terms of convergence and efficient sorting [43], making it the preferred choice for the present work. Figure 7 (c) shows the number of children for each individual using tournament selection method. The selected parents subsequently take part in crossover and mutation operations. The performance of GA also depends on the operators used in the algorithm. Here, adaptive feasible crossover function and uniform mutation functions have been utilized for their inherent advantages. The GA terminates if any of the set stopping criteria (number of generations, time limit, fitness limit and function tolerance) are met. In this work, GA stops after 72 iterations as the average change in fitness value falls below the function tolerance of $1 \times e^{-6}$. Various parameters and functions used in GA are listed in Table 2. For a detailed explanation of the control flow of the GA used to optimize PI controller gains, refer to [44].

4. HESS control strategy with optimized controller parameters

The block diagram in figure 8 illustrates the proposed control strategy, which facilitates coordination among the various units of the MG to minimize deviations in bus voltage and maintain it within specified limits. Balance in generation and load power is maintained regardless of unexpected variations in load cycle and solar irradiance. The primary aim of the control algorithm is to maintain the DC bus voltage at its set value, with the outer control loop generating the gross current necessary to restore this voltage. Gross current is written as

$$I_T^*(t) = k_{p\_v} V_e(t) + k_{i\_v} \int V_e(t) \tag{12}$$

where,

$$V_e(t) = V_{\mathrm{DC}}^*(t) - V_{\mathrm{DC}}(t) \tag{13}$$

and,

$$I_{LF}^*(t) = \frac{1}{1+s\tau} I_T^*(t) \tag{14}$$

here $I_T^*(t)$, is gross injected or required current for the restoration of DC bus voltage. $V_e(t)$ is error in desired and actual DC voltage. In deficit operating mode $I_T^*(t)$ is positive as $V_e(t) > 0$ whereas $I_T^*(t)$ is negative and $V_e(t) < 0$ in excess power mode. The current is passed through a low-pass filter (LPF) and a rate limiter, which restricts charge/discharge rate of battery, to produce the reference current for battery. Reference battery current is than compared to actual battery current and the resulting error signal is processed through a PI controller, which generates PWM signal ($S_{B,1-2}$) for BDCs interlinked to battery and thus minimize error in real time.

High frequency current components along with uncompensated battery power signals are summed up that generate reference current for SC. Reference current for SC is

$$I_{\mathrm{SC}}^* = (I_{\mathrm{HF}}^* - I_{\mathrm{Bat\_error}}) \frac{V_{\mathrm{Bat}}}{V_{\mathrm{SC}}} \tag{15}$$

$$I_{\mathrm{HF}}^* = I_T^* - I_{\mathrm{Bat}}^* \tag{16}$$

The SC's reference current is compared to actual current and fed into a PI controller, which generates duty cycle ($S_{\mathrm{SC},1-2}$) for BDC linked to SC, enabling it to compensate for high fluctuations alongside battery's uncompensated components.

5. Simulation results and discussion

The proposed controlled along with proposed PMS as in figure 8 is tested under the following scenarios. The results as shown in figures 9, 11 and 13 have been discussed subsequently.

Table 2. Parameters and functions used in GA.

parameters	value/function/range
population size	200
iterations	72
crossover function	constraint dependent
selection function	tournament
lower bound [K_{p_B}, K_{i_B}, K_{p_sc}, K_{i_sc}, K_{p_v}, K_{i_v}]	[0.5, 2400, 19, 3000, 0, 700]
upper bound [K_{p_B}, K_{i_B}, K_{p_sc}, K_{i_sc}, K_{p_v}, K_{i_v}]	[1.5, 2800, 22, 3300, 1, 900]

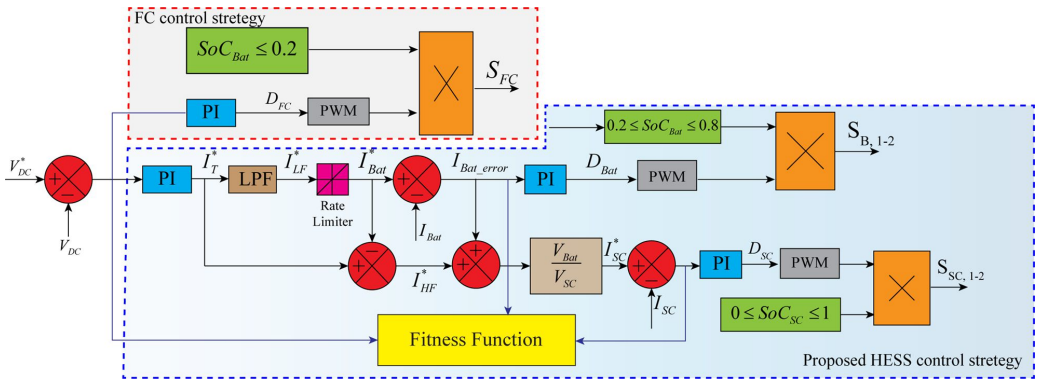

Figure 8. Block diagram of control strategy.

5.1 PV-Battery and SC cogeneration under varying PV irradiance with constant load

This case investigates the scenario when PV-battery and SC maintain the power balance in coordination under constant load conditions. Figure 9 (a) shows a step change in solar irradiance, varying from 255 W/m^2 to 790 W/m^2, while an MPPT controller employing P&O method is utilized to optimize power extraction from PV system.

Figure 9 (b) portrays two operational modes: surplus power mode (SPM) and deficit power mode (DPM), with the DCMG functioning in SPM during the intervals of $1-5$ s and $6-7$ s, when PV generation exceeds load demand. The surplus power generated by PV is injected into the battery and SC. Battery enters into a deeper charging mode, and SC takes care of sudden power demands. Between $0-1$ s and $5-6$ s, the proposed MG configuration is working in the DPM mode as in figure 9 (b). In this mode, PV cannot fulfil the load demands, and thus battery imparts for bridging the gap in steady state while the SC compensates for the unforeseen sudden change in PV generation. Figure 9 (c) shows the time variation of DC bus voltage for conventionally tuned [45] and GA based tuned HESS controllers.

DC bus voltage escalates or diminishes according to quick rise and fall in PV power, which happens due to unforeseen weather conditions. As shown in figure 9 (c), the GA-optimized controller effectively regulates the DC bus

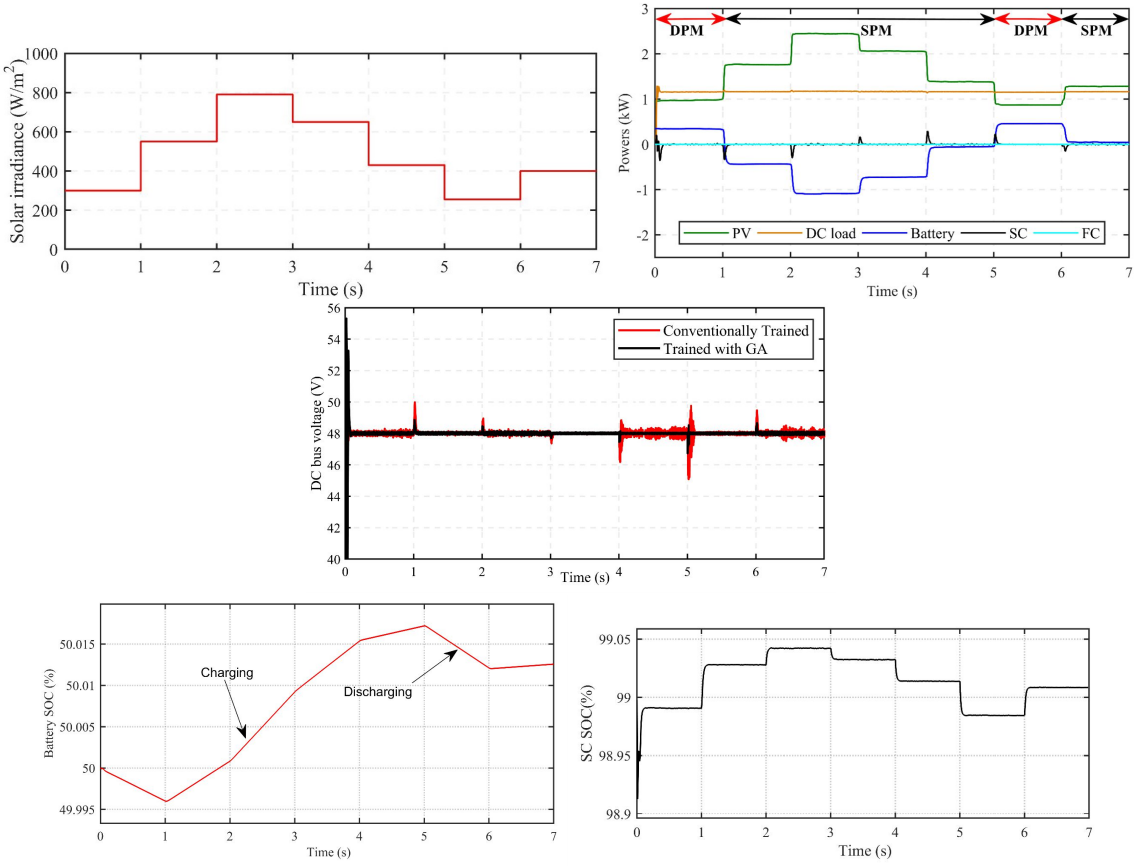

Figure 9. Simulation test results under varying PV irradiation and constant load condition (a) Solar irradiance profile (b) Variation in Power for various units (c) DC bus voltage (d)Battery SoC (e) SC SoC.

voltage, with the maximum undershoot and overshoot occurring at 5 seconds and 6 seconds, reaching acceptable levels of 2.6% and 1.37%, respectively, and always staying within a ±5% range of the desired value.
Figure 9 (d, e) illustrates the trends in SoCs for battery and SC over time, reflecting the different modes of operation. HESS controller decouples slow and quick transients and directs them toward battery and SC. By doing so SC reduces dynamic stresses on battery and thus improves battery life. FC does not participate since the SoC of the battery remains over 20 percent.

5.1.1 Performance comparison

The effectiveness of the proposed HESS controller, depicted in figure 8, is assessed by evaluating settling time, and overshoot/undershoot. The comparison results shown in figure 10, admit superiority of GA tuned HESS controller to conventionally tuned [45] HESS controller for considered performance indices.

5.2 PV-battery and SC cogeneration under varying load conditions

This case examines coordination in the power balance among PV-battery-SC for a time varying load. Solar irradiance and PV temperature are maintained constant at 500 W/m^2 and 25 °C respectively.
PV generates a maximum power of 1778 W continuously at 500 W/m^2 irradiance. It is evident from figure 11 (a),

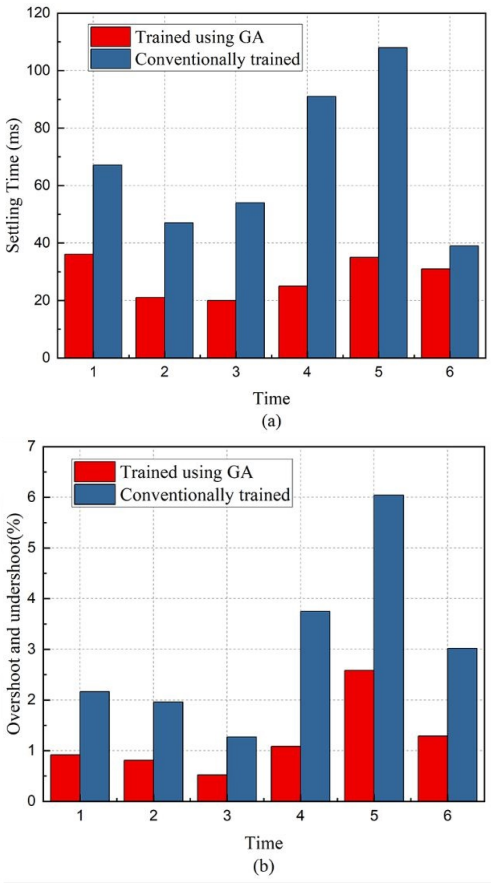

Figure 10. Performance comparison (a) Settling time (b) Overshoot and undershoot (%).

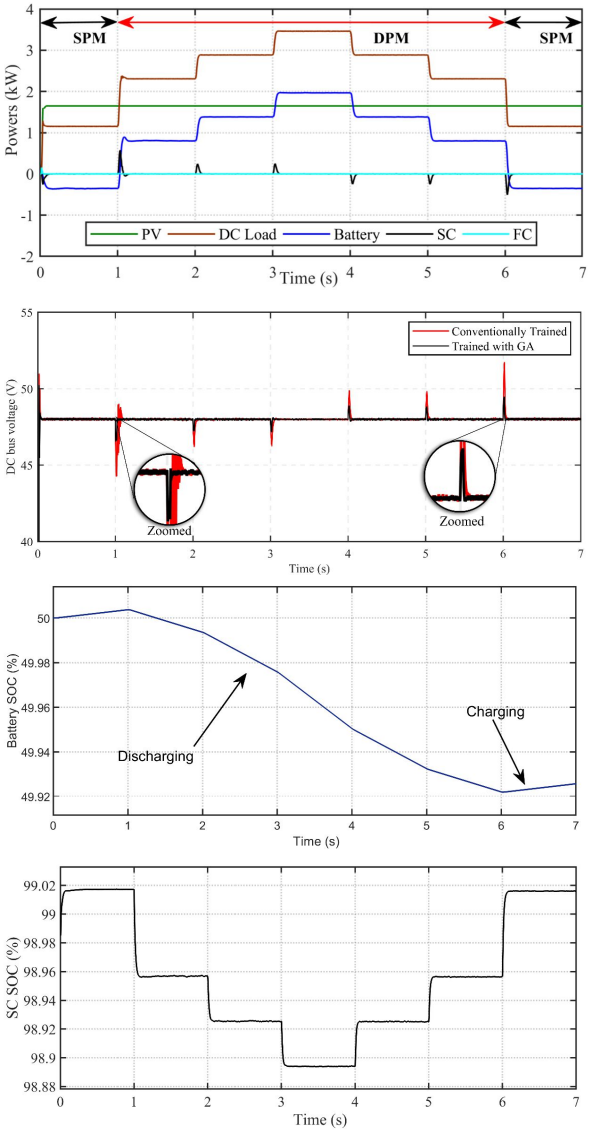

Figure 11. Simulation test results under varying load and constant PV irradiance condition (a) Power sharing among various units (b) DC bus voltage (c) Battery SoC (d) SC SoC.

that the proposed configuration is working under DPM and SPM in intervals $1-6$ s and $0-1$, $6-7$ s, respectively. In DPM, PV power alone is inadequate to fulfil load demand, and battery releases energy to balance power mismatch. SC participates in transient situations and absorbs all dynamic stress according to the control strategy shown in figure 8. In SPM, load demands are less than the power generated by PV alone, as shown in figure 11 (a). This surplus power is injected into the battery for further utilization in case of a power crisis. It is clearly visible in figure 11 (c), that the battery charges during SPM. SC liberates and captures energy whenever sudden increments and decrements in load demands occur. Figure 11 (c, d) shows SoC indices for battery and SC justifying the charging and discharging according to SPM and DPM.
Variation of DC bus voltage for conventionally tuned [45] and GA-based trained HESS controller is highlighted using figure 11 (b). Despite the irregularity in load cycles, the proposed controller in figure 8 effectively regulates the

DC bus voltage, with maximum undershoot and overshoot occurring at 1 second and 6 seconds, reaching acceptable levels of 2.96% and 3.08%, thereby demonstrating that the deviations remain within ±5% of the setpoint value.

5.2.1 Performance comparison

The performance of the proposed HESS controller is evaluated in terms of settling time, as well as overshoot and undershoot, as illustrated in figure 12. It shows that the GA-tuned HESS controllers perform better in comparison to conventional [45] HESS controllers.

5.3 PV-battery, SC and FC cogeneration under varying PV irradiance and load

This case refers to PV-FC and SC maintaining power balance in coordination under DPM and SPM and battery initial SoC is below 20%. Figure 13 (a) shows DPM operation in $1-4$ s intervals while SPM mode in $4-7$ s. In DPM, PV generates power according to varying solar irradiance ranging from 0 W/m^2 to 150 W/m^2 in bad weather conditions. The battery cannot supply power as its SoC lies below 20%. The FC acts as a secondary backup and maintains power balance along with SC while battery remains in idle state. In SPM, PV generates more than load demands as noticed from figure 13 (a) between $4-7$ s. The surplus power is injected into the battery and SC combination. However, SC charge faster due to its faster dynamic response. Surplus power is directed toward battery when SC touches its upper

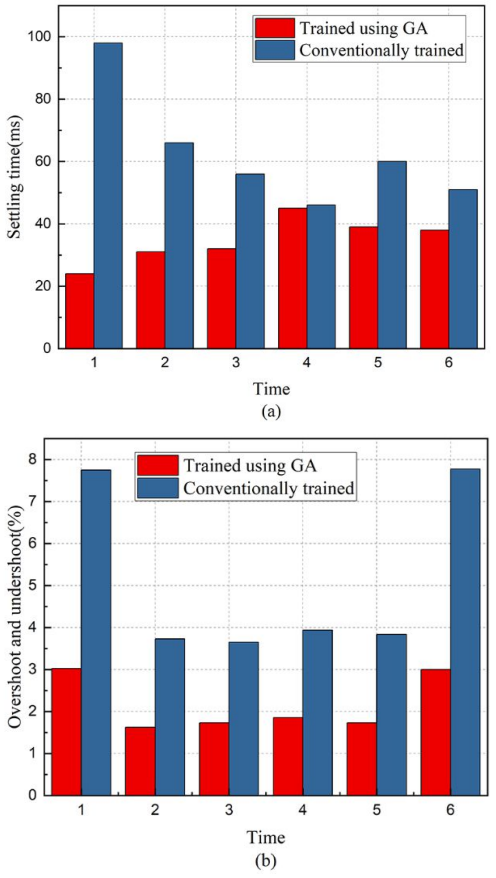

Figure 12. Performance comparison (a) Settling time (b) Overshoot and undershoot (%).

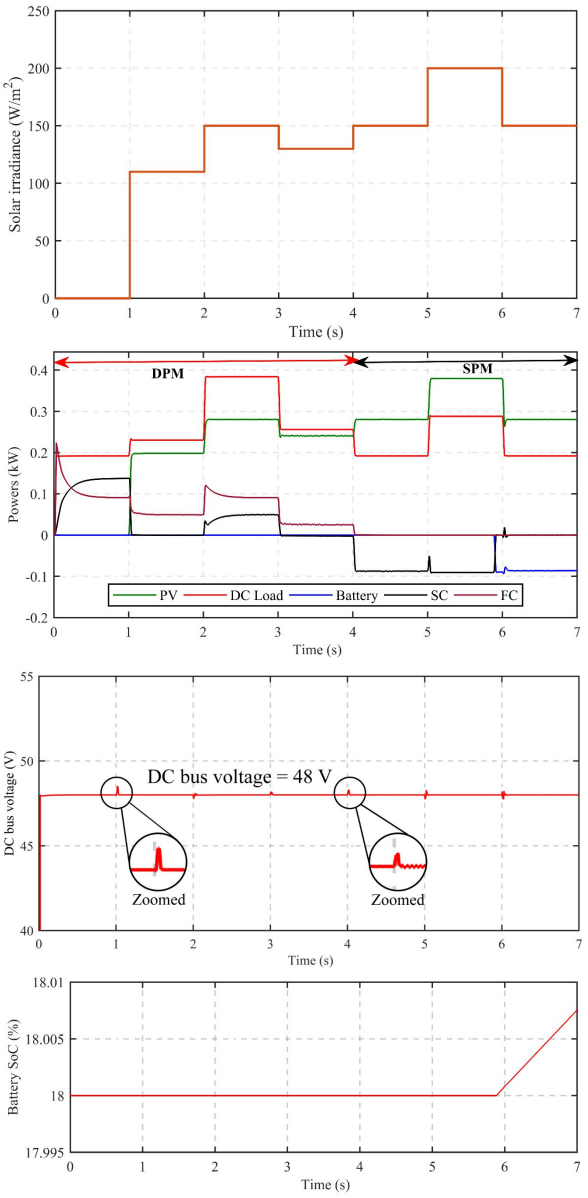

Figure 13. Simulation test results under varying PV irradiance and load (a) Solar irradiance profile (b) Power sharing among various units (c) DC bus voltage (d) Battery SoC.

SoC bound. Figure 13 (c, d) shows DC bus voltage profile in bad weather conditions with disturbance in load cycle and battery SoC respectively.

In this case, the DC bus voltage rapidly reinstates to its set value, with the maximum overshoot and undershoot recorded at 1 second and 5 seconds, reaching 1.06% and 0.52%, respectively.

6. Experimental results and validation

For the proposed MG configuration, illustrated in figure 2, along with the associated controller and PMS, is further validated through a test bench depicted in figure 14. This test bench comprises a host computer, a mixed-signal oscilloscope, and an FPGA-based real-time (RT) simulator (OP 5700). Experimental investigation into all the cases discussed earlier is carried out using an RT simulator, with

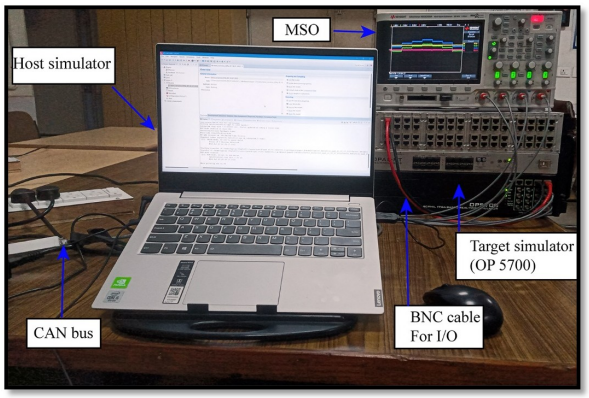

Figure 14. Test bench consisting of host simulator and a real time target (Opal RT 5700).

the results outlined as follows:

6.1 PV-battery and SC cogeneration under varying PV irradiance with constant load

The experimental results presented in figure 15-17 further examine the DC bus VR and power balance, regardless of variations in solar irradiance. From the comparison of figure 9 (b) and figure 15 (b), it is evident that the power balance variations in SPM and DPM scenarios are precisely matching the simulation results, as described, and outlined in section 5.1. This highlights the feasibility of proposed control technique in maintaining power balances and DC bus voltage. Figure 15 (b) depicts two modes of operation i.e., SPM and DPM. In SPM mode, PV generation surpassed the load demand. Thereby, the remaining power is directed towards battery storage. In DPM mode, load demands are higher than the PV generation; hence, to maintain the power balance, battery injects power in all situations, and high frequency fluctuations are diverted towards the SC as shown in figure 15 (b). Thereby, SC stores/releases power when there is sudden rise and fall in solar irradiance level. As a result, high-frequency stresses do not reach the battery, which results in improved life cycles. Figure 15 (b) shows the impacts of solar irradiance on DC bus voltage. The maximum deviation in DC bus voltage is 1.24 V, which is under ±5% of reference voltage of DC bus.

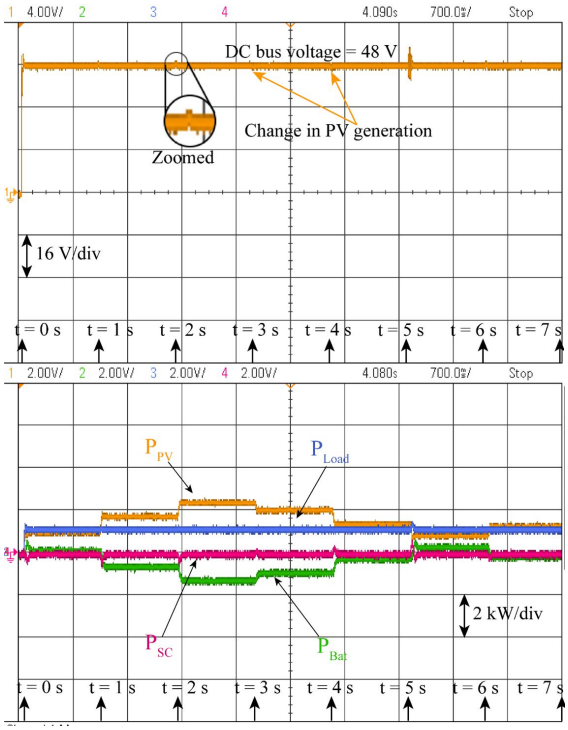

Figure 15. Experimental results under varying PV irradiation and constant load condition (a) DC bus voltage (b) power sharing among various units.

6.2 PV-battery and SC cogeneration under varying load conditions

The experimental study for verifying the simulation results explained and described in section 5.2 has been performed using an RT simulator Op 5700. The RT results are depicted in terms of maintaining power balance among various units and DC bus VR irrespective of sudden load disturbances. As displayed in figure 16 (a), proposed configuration is working in DPM between time interval of $1-6$ s and in SPM, otherwise. In DPM, load power surpasses PV generation, and thus battery provides the necessary support by releasing energy. While in SPM, PV generates more than the demand and thus battery stores surplus power for further utilization. SC plays a crucial role by compensating for high-frequency fluctuation or disturbances in load demand, thus eliminating stress on battery according to the control algorithm shown in figure 8 and thus enhancing battery lifetime. Regulated DC bus voltage waveform is displayed in figure 16 (b). The maximum voltage deviation is 1.45 V, which is as per IEEE standard.

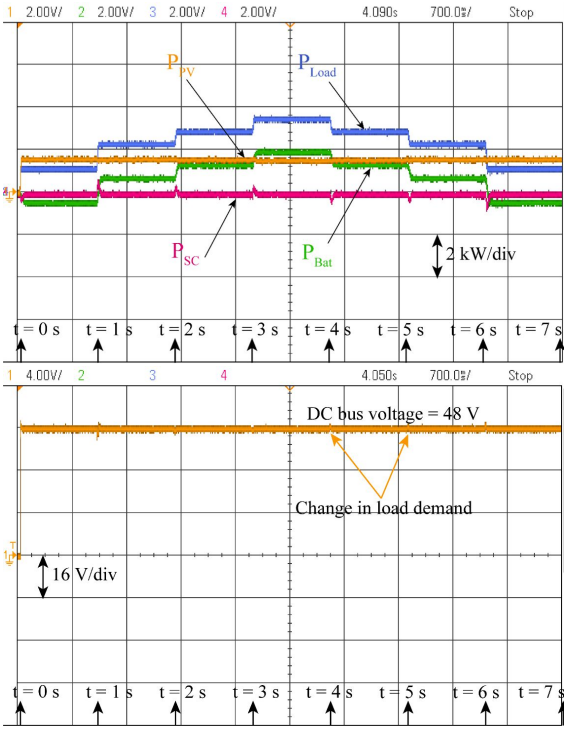

Figure 16. Experimental results under varying load and constant PV irradiance condition (a) Power distribution among various units (b) DC bus voltage.

6.3 PV-battery, SC and FC cogeneration under varying PV irradiance and load

The experimental results for this case depicting load and generation balance in terms of power are shown in figure 17 (a). Experimental results shown in figure 17 (a) portray both DPM and SPM under the situation when battery initial SoC is below 20%. In DPM, PV power along with battery is unable to match power demand required by load. This power deficit is fulfilled through power generation from FC and thus DC bus voltage is restored to its reference value. SC also helps in maintaining power balance and restoration of DC bus voltage due to its fast dynamics. Between 4 – 6 s, PV power is more than load demand i.e., SPM. In this mode, FC is in idle condition while surplus power is stored in battery after SC recharge to its rated voltage. DC bus voltage deviation is very low that can be observed from figure 17 (b).

7. sensitivity analysis

To evaluate robustness of the controller, a simulation study is carried out, in which the system parameters are systematically varied [46]. Three distinct cases of parameter uncertainty are examined to assess the controller's performance under the following conditions:

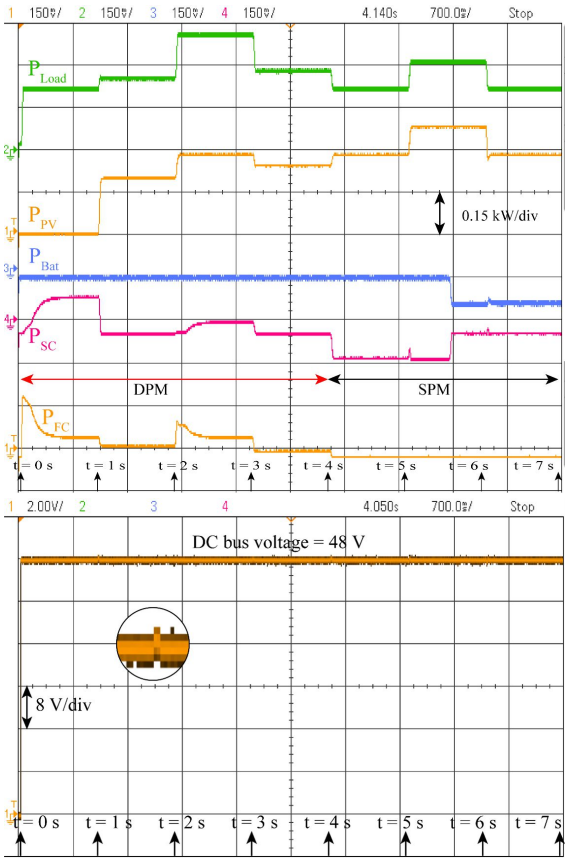

Figure 17. Experimental results under varying PV irradiance and load (a) Power sharing among various units (b) Variation in DC bus voltage.

7.1 Case-I Variation in the inductance of Battery's BDC by ±25 %

7.2 Case-II Variation in the inductance of the SC's BDC by ±25 %

7.3 Case-III Variation in the inductance of PV's converter by ±25 %

Under nominal conditions, the controller gains obtained through GA optimization were preserved while the system parameters were altered to introduce uncertainties for the aforementioned cases. The results presented in figures 18-20 demonstrate that the controller effectively manages

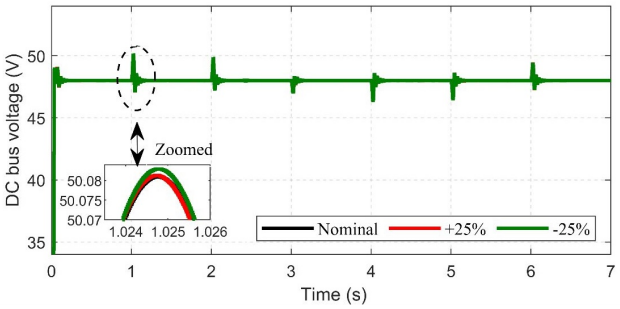

Figure 18. System response for case-I.

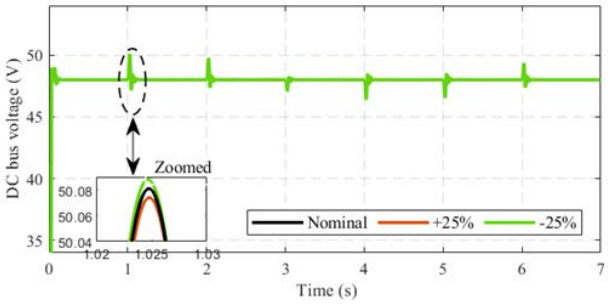

Figure 19. System response for case-II.

parametric uncertainties in a highly robust manner.

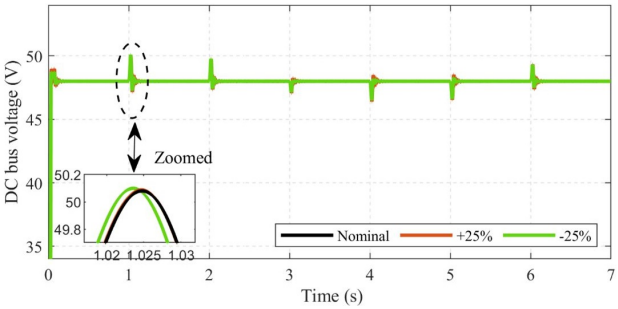

Figure 20. System response for case-III.

8. Performance with sensor noise

The performance of the controllers is evaluated rigorously by analyzing deviations in DC bus voltage. A zero-mean unit variance noise signal, equivalent to 5% of nominal DC bus voltage, is introduced to DC bus voltage sensor to simulate real-world operating conditions, as shown in

figure 21. As shown in figure 22, the proposed controllers demonstrate a robust capability to effectively regulate the DC bus voltage despite the presence of sensor noise. Results indicate that the controller can successfully mitigate the impact of disturbances, thereby enhancing overall system performance.

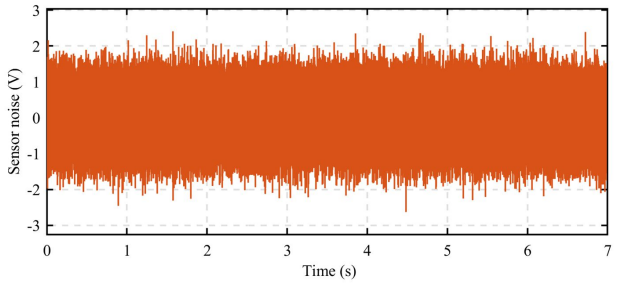

Figure 21. Sensor noise.

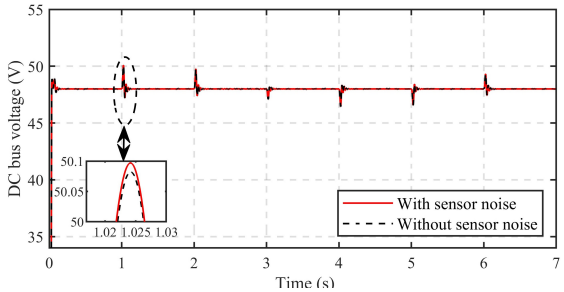

Figure 22. DC bus voltage with and without sensor noise.

9. Future scope

This study provides a pathway for future research to explore additional control strategies, including Model Predictive Control, SMC, and ANFIS, for further enhancing power management in both islanded and grid-connected microgrid configurations.

10. Conclusion

This article presented a GA-tuned PI control strategy for effective power distribution and DC bus VR in a residential MG that integrates RESs and a HESS. The simulation studies demonstrated that the GA-tuned PI controller maintains the DC bus voltage within ±5% of its setpoint, as per IEEE standard 519 – 1992, even under dynamic conditions such as load variations and changes in solar radiation. The control method achieved a maximum overshoot of 3.08%, an undershoot of 2.958%, and a settling time of 44.5ms, highlighting its capability to handle transient scenarios effectively.

The performance evaluation through sensitivity analysis confirmed the robustness of the controllers against parametric variations and sensor noise, showing consistent operation across various conditions. Furthermore, the HIL analysis conducted using OPAL-RT validated the practical reliability of the control strategy, demonstrating strong performance under both steady-state and transient conditions.

Authors Contributions
Authors have contributed equally in preparing and writing the manuscript.

Availability of Data and Materials
The data that support the findings of this study are available from the corresponding author upon reasonable request.

Conflict of Interests
The authors declare that they have no known competing financial interests or personal relationships that could have appeared to influence the work reported in this paper.

References

[1] M. H. Saeed, W. Fangzong, B. A. Kalwar, and S. Iqbal. "**A review on microgrids' challenges & perspectives**.". *IEEE Access*, 9: 166502–166517, 2021.
DOI: https://doi.org/10.1109/ACCESS.2021.3135083.

[2] L. Moosa et al. "**Maldives national adaptation programme**.". *Minist. Environ. Energy Water, 2007*, page 114, 2007. URL https://unfccc.int/resource/docs/napa/mdv01.pdf.

[3] R. K. Chauhan, B. S. Rajpurohit, S. N. Singh, and F. M. Gonzalez-Longatt. "**DC grid interconnection for conversion losses and cost optimization**.". *Springer Verlag*, 0(9789814585262):327–345, 2014.
DOI: https://doi.org/10.1007/978-981-4585-27-9_14/COVER.

[4] J. Stamp and The SPIDERS project. "**Smart power infrastructure demonstration for energy reliability and security at US military facilities**.". *Institute of Electrical and Electronics Engineers (IEEE)*, pages 1–1, 2012.
DOI: https://doi.org/10.1109/ISGT.2012.6175743.

[5] A. K. Rajput and J. S. Lather. "**Energy management and DC bus voltage stabilization in a HRES based DC microgrid using HESS**.". *Serbian J. Electr. Eng*, 20(2):243–268, 2023.
DOI: https://doi.org/10.2298/SJEE2302243R.

[6] D. Kumar, F. Zare, and A. Ghosh. "**DC microgrid technology: System architectures, AC grid interfaces, grounding schemes, power quality, communication networks, ppplications, and standardizations aspects**.". *IEEE Access*, 5:12230–12256, 2017.
DOI: https://doi.org/10.1109/ACCESS.2017.2705914.

[7] Y. Ito, Y. Zhongqing, and H. Akagi. "**DC micro-grid based distribution power generation system**.". *Conference Proceedings - IPEMC 2004: 4th International Power Electronics and Motion Control Conference*, page 1740–1745, 2004.

[8] S. Bandyopadhyay, G. R. C. Mouli, Z. Qin, L. R. Elizondo, and P. Bauer. "**Techno-economical model based optimal sizing of PV-battery systems for microgrids**.". *IEEE Trans. Sustain. Energy*, 11 (3):1657–1668, 2020.
DOI: https://doi.org/10.1109/TSTE.2019.2936129.

[9] M. Alramlawi and P. Li. "**Design optimization of a residential pv-battery microgrid with a detailed battery lifetime estimation model**.". *IEEE Trans. Ind. Appl.*, 56(2):2020–2030, 2020.
DOI: https://doi.org/10.1109/TIA.2020.2965894.

[10] J. J. Caparrós Mancera et al. "**Experimental analysis of the effects of supercapacitor banks in a renewable DC microgrid**.". *Appl. Energy*, 308:118355, 2022.
DOI: https://doi.org/10.1016/J.APENERGY.2021.118355.

[11] F. Zhang et al. "**Power management strategy research for DC microgrid with hybrid storage system**.". *2015 IEEE 1st Int. Conf. Direct Curr. Microgrids, ICDCM 2015*, page 62–68, 2015.
DOI: https://doi.org/10.1109/ICDCM.2015.7152011.

[12] H. Chaouali et al. "**Energy management strategy of a PV/fuel cell/supercapacitor hybrid source feeding an off-grid pumping station modelling and control of systems View project Instrumentation of the fuel cell view project energy management strategy of a PV/Fuel cell/supercapacitor hybrid source feeding an off-grid pumping station**.". *Artic. Int. J. Adv. Comput. Sci. Appl.*, 8(8), 2017.
DOI: https://doi.org/10.14569/IJACSA.2017.080832.

[13] D. B. Wickramasinghe Abeywardana, B. Hredzak, and V. G. Agelidis. "**A fixed-frequency sliding mode controller for a boost-inverter-based battery-supercapacitor hybrid energy storage system**.". *IEEE Trans. Power Electron.*, 32(1):668–680, 2017.
DOI: https://doi.org/10.1109/TPEL.2016.2527051.

[14] L. Maheswari, P. Srinivasa Rao, N. Sivakumaran, G. Saravana Ilango, and C. Nagamani. "**A control strategy to enhance the life time of the battery in a stand-alone PV system with DC loads**.". *IET Power Electron.*, 10(9):1087–1094, 2017.
DOI: https://doi.org/10.1049/IET-PEL.2016.0735.

[15] H. Zhou, T. Bhattacharya, D. Tran, T. S. T. Siew, and A. M. Khambadkone. "**Composite energy storage system involving battery and ultracapacitor with dynamic energy management in microgrid applications**.". *IEEE Trans. Power Electron.*, 26(3):923–930, 2011.
DOI: https://doi.org/10.1109/TPEL.2010.2095040.

[16] G. R. Athira and V. R. Pandi. "**Energy management in islanded DC microgrid using fuzzy controller to improve battery performance**.". *Proceedings of 2017 IEEE International Conference on Technological Advancements in Power and Energy: Exploring Energy Solutions for an Intelligent Power Grid, TAP Energy 2017*, pages 1–6, 2018.
DOI: https://doi.org/10.1109/TAPENERGY.2017.8397369.

[17] Y. Han, W. Chen, Q. Li, H. Yang, F. Zare, and Y. Zheng. "**Two-level energy management strategy for PV-Fuel cell-battery-based DC microgrid**.". *Int. J. Hydrogen Energy*, 44(35):19395–19404, 2019.
DOI: https://doi.org/10.1016/j.ijhydene.2018.04.013.

[18] Y. Pu, Q. Li, W. Chen, and H. Liu. "**Hierarchical energy management control for islanding DC microgrid with electric-hydrogen hybrid storage system**.". *Int. J. Hydrogen Energy*, 4:5153–5161, 2019.
DOI: https://doi.org/10.1016/j.ijhydene.2018.10.043.

[19] Z. Cabrane, D. Batool, J. Kim, and K. Yoo. "**Design and simulation studies of battery-supercapacitor hybrid energy storage system for improved performances of traction system of solar vehicle**.". *J. Energy Storage*, 32:101943, 2020.
DOI: https://doi.org/10.1016/J.EST.2020.101943.

[20] Z. Cabrane, J. Kim, K. Yoo, and M. Ouassaid. "**HESS-based photovoltaic/batteries/supercapacitors: Energy management strategy and DC bus voltage stabilization**.". *Sol. Energy*, 216:551–563, 2021.
DOI: https://doi.org/10.1016/j.solener.2021.01.048.

[21] X. Wen, W. Kai, and Z. Shengzhe. "**Research on hierarchical control strategy of hybrid energy storage system in microgrid**.". *Proceedings - 2017 Chinese Automation Congress, CAC 2017*, page 3323–3326, 2017.
DOI: https://doi.org/10.1109/CAC.2017.8243351.

[22] Y. Han, W. Chen, and Q. Li. "**Energy management strategy based on multiple operating states for a photovoltaic/fuel cell/energy storage DC microgrid**.". *Energies*, 10(1), 2017.
DOI: https://doi.org/10.3390/en10010136.

[23] M. K. Senapati, C. Pradhan, S. R. Samantaray, and P. K. Nayak. "**Improved power management control strategy for renewable energy-based DC micro-grid with energy storage integration**.". *IET Gener. Transm. Distrib.*, 13(6):838–849, 2019.
DOI: https://doi.org/10.1049/iet-gtd.2018.5019.

[24] M. K. Senapati, C. Pradhan, and R. K. Calay. "**A computational intelligence based maximum power point tracking for photovoltaic power generation system with small-signal analysis**.". *Optim. Control Appl. Methods*, 44(2):617–636, 2023.
DOI: https://doi.org/10.1002/OCA.2798.

[25] M. K. Senapati, O. Al Zaabi, K. Al Hosani, K. Al Jaafari, C. Pradhan, and U. R. Muduli. "**Advancing electric vehicle charging ecosystems with intelligent control of DC microgrid stability**.". *IEEE Trans. Ind. Appl.*, 2024.
DOI: https://doi.org/10.1109/TIA.2024.3413052.

[26] M. K. Senapati, K. Al Jaafaari, K. Al Hosani, and U. R. Muduli. "**Flexible control approach for DC microgrid oriented electric vehicle charging station**.". *2023 IEEE IAS Glob. Conf. Renew. Energy Hydrog. Technol.*, 2023.
DOI: https://doi.org/10.1109/GLOBCONHT56829.2023.10087864.

[27] P. Singh and J. S. Lather. "**Design and stability analysis of a control system for a grid-independent direct current microgrid with hybrid energy storage system**.". *Comput. Electr. Eng.*, 93: 107308, 2021.
DOI: https://doi.org/10.1016/J.COMPELECENG.2021.107308.

[28] A. K. Rajput and J. S. Lather. "**Energy management of a DC microgrid with hybrid energy storage system using PI and ANN based hybrid controller**.". *Int. J. Ambient Energy*, 44(1):703–718, 2023.
DOI: https://doi.org/10.1080/01430750.2022.2142285.

[29] D. Pavković, M. Lobrović, M. Hrgetić, and A. Komljenović. "**A design of cascade control system and adaptive load compensator for battery/ultracapacitor hybrid energy storage-based direct current microgrid**.". *Energy Convers. Manag.*, 114:154–167, 2016.
DOI: https://doi.org/10.1016/J.ENCONMAN.2016.02.005.

[30] J. W. Umland and M. Safiuddin. "**Magnitude and symmetric optimum criterion for the design of linear control systems: What is it and how does it compare with the others?**.". *IEEE Trans. Ind. Appl.*, 26(3):489–497, 1990.
DOI: https://doi.org/10.1109/28.55967.

[31] D. Vranči, S. Strmčnik, and A. Juriči. "**A magnitude optimum multiple integration tuning method for filtered PID controller**.". *Automatica*, 37(9):1473–1479, 2001.
DOI: https://doi.org/10.1016/S0005-1098(01)00088-7.

[32] L. Fan and E. M. Joo. "**Design for auto-tuning PID controller based on genetic algorithms**.". *2009 4th IEEE Conf. Ind. Electron. Appl. ICIEA 2009*, page 1924–1928, 2009.
DOI: https://doi.org/10.1109/ICIEA.2009.5138538.

[33] T. Praveen Kumar, N. Subrahmanyam, and S. Maheswarapu. "**Genetic algorithm based power control strategies of a grid integrated hybrid distributed generation system**.". *Technol. Econ. Smart Grids Sustain. Energy*, 6(1):1–14, 2021.
DOI: https://doi.org/10.1007/S40866-021-00109-8/TABLES/2.

[34] M. Y. El-Sharkh, A. Rahman, M. S. Alam, P. C. Byrne, A. A. Sakla, and T. Thomas. "**A dynamic model for a stand-alone PEM fuel cell power plant for residential applications**.". *J. Power Sources*, 138(1-2):199–204, 2004.
DOI: https://doi.org/10.1016/j.jpowsour.2004.06.037.

[35] S. G. Malla and C. N. Bhende. "**Voltage control of stand-alone wind and solar energy system**.". *Int. J. Electr. Power Energy Syst.*, 56:361–373, 2014.
DOI: https://doi.org/10.1016/j.ijepes.2013.11.030.

[36] O. Tremblay and L. A. Dessaint. "**Experimental validation of a battery dynamic model for EV applications**.". *World Electr. Veh. J.*, 3(2):289–298, 2009.
DOI: https://doi.org/10.3390/wevj3020289.

[37] K. B. Oldham. "**A Gouy–Chapman–Stern model of the double layer at a (metal)/(ionic liquid) interface**.". *J. Electroanal. Chem.*, 613(2):131–138, 2008.
DOI: https://doi.org/10.1016/J.JELECHEM.2007.10.017.

[38] D. Somwanshi, M. Bundele, G. Kumar, and G. Parashar. "**Comparison of fuzzy-PID and PID controller for speed control of DC motor using LabVIEW**.". *Procedia Computer Science*, page 252–260, 2019.
DOI: https://doi.org/10.1016/j.procs.2019.05.019.

[39] J. G. Ziegler and N. B. Nichols. "**Optimum settings for automatic controllers**.". *J. Dyn. Syst. Meas. Control*, 115(2B):220–222, 1995.
DOI: https://doi.org/10.1115/1.2899060.

[40] C. G. A. Cohen G. H. "**Theoritical considerations of retarded control**.". *Trans. ASME*, 75(5):827–834, 1953.
DOI: https://doi.org/10.1115/1.4015451.

[41] L. Hao, C. Ma, and F. Li. "**Study of adaptive PID controller based on single neuron and genetic optimization**.". *2007 8th International Conference on Electronic Measurement and Instruments, ICEMI*, page 1240–1243, 2007.
DOI: https://doi.org/10.1109/ICEMI.2007.4350432.

[42] L. Junli, M. Jianlin, and Z. Guanghui. "**Evolutionary algorithms based parameters tuning of PID controller**.". *Proceedings of the 2011 Chinese Control and Decision Conference, CCDC 2011*, page 416–420, 2011.
DOI: https://doi.org/10.1109/CCDC.2011.5968215.

[43] Y. S. Lata and S. Asha. "**Comparative study of different selection techniques in genetic algorithm**.". *Int. J. Eng. Sci. Math.*, 6(3): 174–180, 2017.

[44] A. A. Aly. "**PID parameters optimization using genetic algorithm technique for electrohydraulic servo control system**.". *Intell. Control Autom*, 02(02):69–76, 2011.
DOI: https://doi.org/10.4236/ica.2011.22008.

[45] S. Punna, R. Mailugundla, and S. R. Salkuti. "**Design, analysis and implementation of bidirectional DC–DC converters for HESS in DC microgrid applications**.". *Smart Cities 2022, Vol. 5, Pages 433-454*, 5(2):433–454, 2022.
DOI: https://doi.org/10.3390/SMARTCITIES5020024.

[46] N. Saini and J. Ohri. "**Optimal load frequency control of a multi-area power system with dead band effect and generation rate constraints**.". *Majlesi J. Electr. Eng.*, 17(1):81–96, 2023.
DOI: https://doi.org/10.30486/MJEE.2023.1970197.0.